Static condensation method for the reduced dynamic modeling of mechanisms and structures

Alessandro Cammarata, Rosario Sinatra & Pietro Davide Maddìo

Archive of Applied Mechanics

ISSN 0939-1533
Volume 89
Number 10

Arch Appl Mech (2019) 89:2033-2051
DOI 10.1007/s00419-019-01560-x

00419

Volume 89 · Issue 10 · October 2019

Archive of Applied Mechanics

Springer

Springer

Arch Appl Mech (2019) 89:2033–2051
https://doi.org/10.1007/s00419-019-01560-x

ORIGINAL

Alessandro Cammarata · Rosario Sinatra · Pietro Davide Maddìo

Static condensation method for the reduced dynamic modeling of mechanisms and structures

Received: 3 December 2018 / Accepted: 7 May 2019 / Published online: 15 May 2019

Abstract In this paper, a novel static condensation method is extended to mechanisms and structures with internal joints. The formulation is framed inside the static reduction techniques in a similar way to the classic Guyan–Iron reduction. A new class of joint nodes is added to the existing classes of inner and boundary nodes to consider joint constraints inside the compatibility conditions. Within the set of joint nodes, a reduced subset of independent nodes can be individuated to perform the static reduction. A simple connection rule is provided to determine the independent nodes of a mechanical system composed of rigid bodies, flexible components and joints. The inner and boundary nodes are then expressed in terms of the independent joint nodes to form a new transformation matrix able to reduce the stiffness and mass matrices of the original system without connections. Joint stiffness and external forces are also included in the final reduction process. Finally, two examples prove the efficiency and demonstrate the equivalence and compatibility of the proposed method with other static reduction techniques in order to create a unique substructuring framework.

Keywords Static reduction · Substructuring techniques · Low-order models

1 Introduction

The *static condensation methods* are reduction techniques that consider only the first-order approximation of the exact reduced eigenproblem. These simplified formulations are used to overcome the computational complexity introduced by other dynamic reduction methods and must be applied carefully to avoid gross errors and low accuracy of results. The Guyan–Iron (GI) method [13] is the most known static reduction method, in which the inner nodes of FE models are statically reduced to boundary nodes. The GI method is exact for static problems, but it does not succeed in reducing a system without damaging its dynamical properties: In particular, its accuracy strongly depends on the choice and number of the boundary nodes describing the final reduced system [23]. Quasistatic GI condensation or Higher-Order GI condensation [11] tend to increase the accuracy, shifting the frequency of reference or considering more terms in the power series of the dynamic flexible matrix.

Other well-established substructuring methods are based on the *Component Mode Synthesis* (CMS) [10,14,15,17]. These methods rely on the *Ritz basis* assumption to express structure displacements as a combination of mode sets. When this basis takes into account an infinite number of terms obtained by the power expansion of the flexibility matrix, the associated method is said *exact*. The word "exact" refers to the closed-form solution of the equations of motions without introducing displacement approximations or reduced models and reproduces

A. Cammarata (✉) · R. Sinatra · P. D. Maddìo
Dipartimento Ingegneria Civile e Architettura, University of Catania, Via Santa Sofia, 54, 95125 Catania, Italy
E-mail: alessandro.cammarata@unict.it
Tel.: +39 0957382403
Fax: +39 0950932873

the displacement field for any frequency [19,22,29]. Different CMS methods are classified according to how they handle interface compatibility: Methods with *fixed* interface [16] and with *free* interface modes [20,25] are among the most common. In a reduced model, the slave nodes are usually more than the boundary nodes and the dimension of the dynamic flexibility matrix might be large, making the exact computation expensive.

The proposed approach overcomes some limitations of our previous formulations developed in [1,4–8], related to the classification of parts. The new formulation does not require either classifications or an order in the couplings. Furthermore, the boundary conditions can be directly included in the definition of the joint compatibility conditions, therefore, avoiding manual operations to delete the *dofs* of the fixed nodes. Following the *linear structural dynamics*, our approach combines FE/MSA (Matrix Structural Analysis) techniques and considers already linearized equations in the neighborhood of a local configuration. The nonlinear holonomic constraints are substituted by linear constraints expressed in terms of small displacements and rotations. Subsequently, a projection operation, with linear operators orthogonal to the local joint space, is used to condense the joint variables without resorting to the use of Lagrange multipliers. We point out that the proposed approach is different and cannot be compared to the nonlinear methods used in flexible multibody systems. The reader is referred to specific books and papers for further information [3,9,12,18,21,26–28].

The rest of the paper is organized as follows. In Sect. 2, the Guyan–Iron method is first recalled to better understand the differences and similarities with the proposed method. In Sect. 3, the new class of *joint nodes* is first introduced. Stiffness and mass matrices of the mechanical system without connections are partitioned into blocks and referred to inner and boundary nodes. The joint nodes are then used to define the joint constraints: In particular, each joint yields a vector equation in which the displacements of a joint node are expressed in terms of the displacements of a reduced set of independent joint nodes. A simple connection rule is provided to select the independent joint nodes necessary to reduce the system finding a static transformation matrix similar to that obtained using the Guyan–Iron method. In Sect. 4, the method is first applied to a two-beam frame chosen as a benchmark example. Comparison to classic Guyan reduction is addressed, and three models are compared to commercial software for validation. Then, the case study of the Ragnar robot is investigated. The model of one leg is accurately described using both flexible and rigid parts to help the reader to understand different modeling strategies. The actuator stiffness is added to the actuated revolute joints of the base platform. Besides, the reduced stiffness and mass matrices, the latter including also lumped mass/inertia, are obtained. Finally, a second static reduction is applied to find the Cartesian matrices at the end-effector point.

2 Guyan–Iron static reduction

In this section, the Guyan–Iron method [13] is recalled to better introduce the reader to the following sections. In the Guyan–Iron method, two types of nodes are considered: the inner or "slave" nodes, denoted with subscript *i*, and the boundary or "master" nodes, labeled with subscript *b*. Usually, the boundary nodes are interface nodes that connect a subsystem to other subsystems. Furthermore, they can include nodes of particular interest or nodes where external loads are applied. By contrast, the inner nodes are internal nodes of the structure. The Guyan–Iron method employs a static reduction, in which the inner nodes are condensed and expressed in terms of the boundary nodes.

In the following description, the node displacement vector $\mathbf{u}$ will contain three linear displacements, namely s_x, s_y, and s_z, along three coordinate axes and three small angular rotations, indicated by ϕ_x, ϕ_y, and ϕ_z, around the same axes. Consider the linearized dynamic system expressed in terms of the global displacement vectors $\mathbf{u}_\mathrm{I}$ and $\mathbf{u}_\mathrm{B}$ of inner and boundary nodes, respectively:

$$\begin{bmatrix} \mathbf{M}_\mathrm{II} & \mathbf{M}_\mathrm{IB} \\ \mathbf{M}_\mathrm{BI} & \mathbf{M}_\mathrm{BB} \end{bmatrix} \begin{bmatrix} \ddot{\mathbf{u}}_\mathrm{I} \\ \ddot{\mathbf{u}}_\mathrm{B} \end{bmatrix} + \begin{bmatrix} \mathbf{K}_\mathrm{II} & \mathbf{K}_\mathrm{IB} \\ \mathbf{K}_\mathrm{BI} & \mathbf{K}_\mathrm{BB} \end{bmatrix} \begin{bmatrix} \mathbf{u}_\mathrm{I} \\ \mathbf{u}_\mathrm{B} \end{bmatrix} = \begin{bmatrix} \mathbf{0} \\ \mathbf{f}_\mathrm{B} \end{bmatrix} \tag{1}$$

where the following notation has been used:

- $\mathbf{f}_\mathrm{B}$: vector of external forces applied to the boundary nodes,
- $\mathbf{M}_{KL}$: partitioned block of the mass matrix,
- $\mathbf{K}_{KL}$: partitioned block of the stiffness matrix.

The Guyan–Iron method considers only the static terms of Eq. (1) to carry out the static reduction; therefore,

$$\begin{bmatrix} \mathbf{K}_\mathrm{II} & \mathbf{K}_\mathrm{IB} \\ \mathbf{K}_\mathrm{BI} & \mathbf{K}_\mathrm{BB} \end{bmatrix} \begin{bmatrix} \mathbf{u}_\mathrm{I} \\ \mathbf{u}_\mathrm{B} \end{bmatrix} = \begin{bmatrix} \mathbf{0} \\ \mathbf{f}_\mathrm{B} \end{bmatrix} \tag{2}$$

From the first equation of system (2), $\mathbf{u}_\mathrm{I}$ can be expressed in terms of $\mathbf{u}_\mathrm{B}$, i.e.,

$$\mathbf{K}_\mathrm{II}\mathbf{u}_\mathrm{I} + \mathbf{K}_\mathrm{IB}\mathbf{u}_\mathrm{B} = \mathbf{0} \Rightarrow \mathbf{u}_\mathrm{I} = -\mathbf{K}_\mathrm{II}^{-1}\mathbf{K}_\mathrm{IB}\mathbf{u}_\mathrm{B} \tag{3}$$

Using the previous expression, the static transformation matrix Ψ can be defined:

$$\begin{bmatrix} \mathbf{u}_\mathrm{I} \\ \mathbf{u}_\mathrm{B} \end{bmatrix} = \Psi \mathbf{u}_\mathrm{B} \Rightarrow \Psi = \begin{bmatrix} -\mathbf{K}_\mathrm{II}^{-1}\mathbf{K}_\mathrm{IB} \\ \mathbf{1} \end{bmatrix} \tag{4}$$

The matrix Ψ does not depend on time and is used to transform the dynamic system (1) into its reduced form, i.e.,

$$\mathbf{M}_\mathrm{G}\ddot{\mathbf{u}}_\mathrm{B} + \mathbf{K}_\mathrm{G}\mathbf{u}_\mathrm{B} = \mathbf{F}_\mathrm{B} \tag{5}$$

where "G" stands for Guyan and $\mathbf{M}_\mathrm{G}$, $\mathbf{K}_\mathrm{G}$ and $\mathbf{F}_\mathrm{B}$, respectively, are the reduced mass and stiffness matrices, and the reduced force vector, respectively, defined as

$$\mathbf{M}_\mathrm{G} = \Psi^\mathrm{T}\mathbf{M}\Psi, \quad \mathbf{K}_\mathrm{G} = \Psi^\mathrm{T}\mathbf{K}\Psi, \quad \mathbf{F}_\mathrm{B} = \Psi^\mathrm{T}\mathbf{f}_\mathrm{B} \tag{6}$$

or in extended form:

$$\mathbf{K}_\mathrm{G} \equiv \mathbf{K}_\mathrm{BB} - \mathbf{K}_\mathrm{BI}\mathbf{K}_\mathrm{II}^{-1}\mathbf{K}_\mathrm{IB} \tag{7a}$$

$$\mathbf{M}_\mathrm{G} \equiv \mathbf{M}_\mathrm{BB} - \mathbf{K}_\mathrm{BI}\mathbf{K}_\mathrm{II}^{-1}\mathbf{M}_\mathrm{II}\mathbf{K}_\mathrm{II}^{-1}\mathbf{K}_\mathrm{IB} - \mathbf{K}_\mathrm{BI}\mathbf{K}_\mathrm{II}^{-1}\mathbf{M}_\mathrm{IB} - \mathbf{M}_\mathrm{BI}\mathbf{K}_\mathrm{II}^{-1}\mathbf{K}_\mathrm{IB} \tag{7b}$$

$$\mathbf{F}_\mathrm{B} \equiv \mathbf{f}_\mathrm{B} \tag{7c}$$

The Guyan–Iron is one of the simplest reduction methods used in substructuring techniques since it does not consider dynamic forces. Unfortunately, its accuracy strongly depends on the boundary nodes definition. Indeed, the reliability of the reduced model is highly depending on the number and/or the location of the boundary nodes.

3 Static reduction in multibody systems

This section is composed of three subsections describing the general formulation to obtain a static reduction in mechanical systems with internal connections. The formulation can be applied to study the linear elastodynamics of multibody systems and structures with joints. In Sect. 3.1, the new class of joint nodes is first introduced. Then, the independent nodes are selected using the connection rule. In Sect. 3.2, the rigid and moving connections are first described, and then, their mathematical formulation in terms of constraints is provided. Finally, in Sect. 3.3 the novel static transformation for multibody systems is derived.

3.1 Classifying nodes

As already highlighted, substructuring methods are generally used to reduce the size of individual components that are then joined to form bigger structures. In the absence of joints, the assembly is performed combining the interface nodes of different substructures, that is merging the corresponding boundary nodes of the substructures to be assembled.

When two sub-parts must be combined through a joint, a constraint is created between the corresponding boundary nodes that are involved in the connection and that belong to the two sub-parts. In the so-called *primal assembly*, the constraint is expressed in terms of displacements; in the *dual assembly*, the constraint is enforced using constraint forces [24]. In the following, we will refer only to the primal assembly and all constraint equations will be written in terms of displacements. Constraints are mathematically expressed by means of equations or inequalities connecting several variables to each other. This means that the variables are no longer independent, but there is a bond that allows expressing a variable in terms of others, chosen as independent variables. For our purposes, all of this means that two boundary nodes connected through a joint cannot both be independent. It is noteworthy that this is not the case for the previous Guyan–Iron method, in which all the inner nodes are dependent and all the boundary nodes are independent.

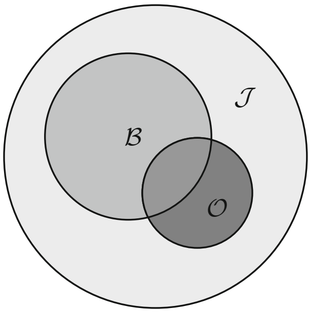

Fig. 1 Node sets: $\mathcal{B}$—boundary nodes, $\mathcal{J}$—joint nodes, $\mathcal{O}$—independent joint nodes

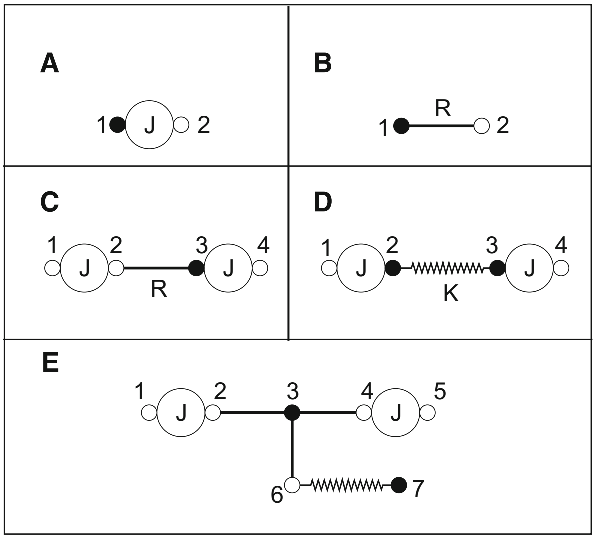

Fig. 2 Rules to define the independent nodes: The independent nodes are reported with filled circles; the dependent nodes are represented with blank circles; J is the generic joint; R is the rigid connection; K represents a flexible component

In order to describe the joint constraints, the set $\mathcal{I}$ of inner nodes and the set $\mathcal{B}$ of boundary nodes must be complemented with the introduction of a new set $\mathcal{J}$ of *joint nodes* which includes all nodes subject to joint constraints. Since the inner nodes are internal to the sub-parts, the sets $\mathcal{J}$ and $\mathcal{I}$ are separated and their intersection is the null set $\varnothing$, i.e., $\mathcal{J} \cap \mathcal{I} = \varnothing$. Furthermore, as shown in Fig. 1, the set $\mathcal{J}$ includes the set $\mathcal{B}$ of boundary nodes. The remaining set $\mathcal{O}$ displayed in Fig. 1 is a particular subset of independent joint nodes. It can be observed that $\mathcal{O}$ may intersect $\mathcal{B}$ meaning that the set of independent joint nodes can or cannot contain boundary nodes. The set $\mathcal{O}$ of independent joint nodes is crucial for the proposed formulation, and our scope in this subsection is that to discover its dimension and the nodes that compose it. In order to find the dimension $n_{\mathcal{O}}$ of $\mathcal{O}$, the concept of *connection* must be introduced. A connection imposes a displacement constraint to one or between two or more nodes and can be of three types: rigid, mobile, and imposed. The rigid and mobile connections involve two or more nodes, while the imposed connection is usually applied to single nodes. As shown in the boxes A and B of Fig. 2, a mechanical joint J is a mobile connection, whereas a rigid-body constraint R is a rigid connection. The last type of imposed connection pertains to displacements or boundary conditions imposed to specific nodes, e.g., the fixed nodes of a mechanism or structure.

The dimension $n_{\mathcal{O}}$ of $\mathcal{O}$ can be evaluated considering the dimension $n_{\mathcal{J}}$ of $\mathcal{J}$ and the number of connections n_c, i.e.,

$$n_{\mathcal{O}} = n_{\mathcal{J}} - n_c \tag{8}$$

The independent nodes are selected according to the following simple rule:

Definition 1 (*Connection rule*) rigid and mobile connections involve **at most** one independent node. All nodes with imposed connections are independent.

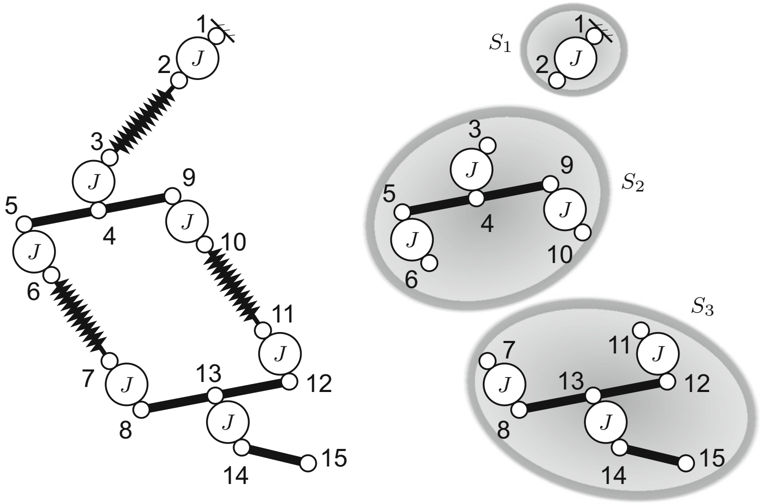

Fig. 3 Leg of the Ragnar robot: (left)—general layout; (right)—subsystems S_i, $i = 1, 2, 3$

From the *connection rule*, it follows that:

Remark 1 (Rigid connection:) if several joint nodes belong to a rigid body, at most only one of these can be independent.

The box C reports four nodes coupled by means of two joints and a rigid connection. The three connections create three constraints between the four nodes that make three nodes dependent on the fourth chosen as independent. As a matter of fact, using the *connection rule* only one node can be chosen as independent.

Flexible parts, or more generally elastic couplings, are not considered connections since they impose force constraints and not displacement constraints between two or more nodes. It is suggested to cut each elastic coupling and calculate the independent nodes separately in each subsystem. In fact, each subsystem must comply with the *connection rule* and the number of independent nodes must be calculated using Eq. (8).

The box D shows a four-node system composed of two joints and a flexible part K, enclosed between its boundary nodes 2 and 3. In this case, cutting the elastic coupling two subsystems are identified: The first subsystem is composed of node 1 and 2, and the second subsystem is composed of node 3 and 4. For each of the two subsystems, it is possible to define only one independent node at this point.

Finally, in box E a more complicated seven-node system is shown. In this case, the system is composed of seven joint nodes coupled through three rigid connections R, two mobile connections J, and one elastic coupling K. Cutting the elastic coupling two subsystems are identified. The first subsystem includes only the node 7 that is chosen as the first independent node. The joint nodes from 1 to 6 form the second subsystem. The latter follows the same rule of box C; therefore: $n_{\mathcal{O}} = n_{\mathcal{J}} - n_c \Rightarrow n_{\mathcal{O}} = 6 - 5 \equiv 1$, meaning that only one node can be selected as the second independent node.

We finally report the system that will be used in Sect. 4.2 to model one leg of the Ragnar robot. As shown in Fig. 3, the generic leg is a complex system composed of 15 joint nodes, 5 rigid connections R, 7 mobile connections J, 3 flexible couplings K, and 1 imposed connection to node 1. By applying Eq. (8), we derive that the system has two independent nodes, i.e., $n_{\mathcal{O}} = n_{\mathcal{J}} - n_c \Rightarrow n_{\mathcal{O}} = 15 - 13 \equiv 2$. In order to select these two nodes, we must ensure that every subsystem in which the leg is divided fulfills the connection rule. Therefore, cutting the flexible couplings the three subsystems S_i, $i = 1, 2, 3$ outlined in the right side of Fig. 3 are individuated. Starting from the first subsystem S_1, the first node has an imposed displacement and, according to the connection rule, must be selected as an independent node. Since node 1 is constrained to be fixed, its displacements are zero and the node is removed from the set $\mathcal{O}$ of independent nodes. In the second subsystem S_2, only one independent node can be selected, i.e., $n_{\mathcal{O}} = n_{\mathcal{J}} - n_c \Rightarrow n_{\mathcal{O}} = 6 - 5 \equiv 1$. Finally, for the third subsystem S_3 it stands that $n_{\mathcal{O}} = n_{\mathcal{J}} - n_c \Rightarrow n_{\mathcal{O}} = 7 - 6 \equiv 1$. Further details will be provided in Sect. 4.2.

To sum up, the number $n_{\mathcal{O}}$ of independent nodes is determined using Eq. (8). The selection of the independent nodes is determined by the designer, but his choice must comply with the *connection rule*. In the following list, we recall the steps needed to select the independent nodes of a mechanical system or a structure with rigid bodies, flexible components, and joints:

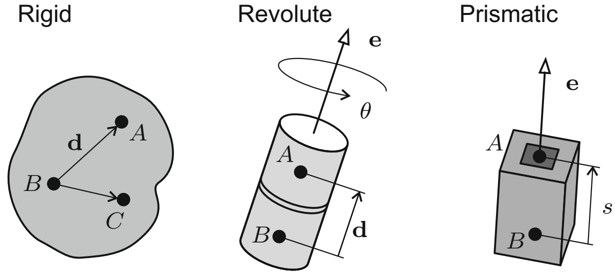

Fig. 4 Rigid connection and mobile connections: prismatic and revolute joints

1. Individuate the joint nodes of the mechanism,
2. Find the rigid, mobile, and imposed connections of the system,
3. Cut the flexible couplings and identify all subsystems,
4. Find the number n_O of independent nodes of each subsystem by means of Eq. (8),
5. Select the independent nodes of each subsystem using the *connection rule*.

3.2 Connections type

In the previous subsection, the number and type of independent joint nodes of a system in the presence of connections have been determined. Here, we provide a mathematical description of the connections expressed in terms of constraint equations involving displacements.

The first connection that we describe is the rigid connection. Referring to the left box of Fig. 4, when two joint nodes A and B are coupled by means of a rigid connection their distance must remain unchanged. In terms of displacements, the displacements of node A can be expressed using the displacements of the other node B using the following expression:

$$\mathbf{u}_j^A = \mathbf{G}_j(\mathbf{d})\mathbf{u}_j^B \tag{9}$$

where $\mathbf{d}$ is the distance vector going from node B to node A and $\mathbf{G}_j(\mathbf{d})$ is the 6 × 6 rigid-body transformation matrix, defined as

$$\mathbf{G}_j(\mathbf{d}) = \begin{bmatrix} \mathbf{1} & -\mathbf{D} \\ \mathbf{O} & \mathbf{1} \end{bmatrix} \tag{10}$$

with $\mathbf{D}$ skew-symmetric matrix, or cross-product matrix, of $\mathbf{d}$, [2]. Considering another node C, belonging to the same rigid body, it will be possible to express $\mathbf{u}_j^C$ in function of $\mathbf{u}_j^B$ as in Eq. (9). This statement confirms the remark of the previous subsection which states that in a rigid body only one node can be chosen as independent.

When two nodes, say A and B, are coupled by means of a mobile connection, the rigid-body transformation (9) must be augmented considering the displacements $\boldsymbol{\theta}_m$ permitted by the joint. The vector of joint displacements $\boldsymbol{\theta}_m$ depends on the type of joint and can include translations and/or rotations as vector components. Furthermore, the joint displacements will take place along or around some geometric features, i.e., unit vectors, characteristic of the type of joint taken into consideration. These features are collected within a matrix, referred to as the *joint matrix* $\mathbf{H}$, that will be used to write the joint constraints. As relevant cases, below we report the revolute and prismatic joints; all other joints can be built by combining these two fundamental cases.

Figure 4 shows a revolute joint and a prismatic joint along with the corresponding geometric features. The two joint nodes A and B, respectively, belong to each of the two kinematic pairs in which the joint can be divided. For the revolute joint, the displacement vector $\mathbf{u}_A$ can be expressed as

$$\mathbf{u}_j^A = \mathbf{G}_j(\mathbf{d})\mathbf{u}_j^B + \mathbf{h}_j\theta_m, \quad \mathbf{h}_j = \begin{bmatrix} \mathbf{0}^{\mathrm{T}} & \mathbf{e}^{\mathrm{T}} \end{bmatrix}^{\mathrm{T}} \tag{11}$$

The six-dimensional vector $\mathbf{h}_j$ contains the geometric feature of the revolute joint. It is noteworthy that $\mathbf{e}$ is present only in the rotational part of $\mathbf{h}_j$ because the revolute joint allows only for a relative rotation about its revolute axis. For the prismatic joint, it stands that

$$\mathbf{u}_j^A = \mathbf{G}_j(\mathbf{d})\mathbf{u}_j^B + \mathbf{h}_j s, \quad \mathbf{h}_j = \begin{bmatrix} \mathbf{e}^{\mathrm{T}} & \mathbf{0}^{\mathrm{T}} \end{bmatrix}^{\mathrm{T}} \tag{12}$$

In this case, the unit vector $\mathbf{e}$ is present only in the translational part of $\mathbf{h}_j$. Notice that the rigid-body transformation $\mathbf{G}_j(\mathbf{d})$ becomes the 6 × 6 identity matrix if the two nodes occupy the same position in space, i.e., $\mathbf{d} = \mathbf{0}$. More complex joints can be created assembling several revolute and prismatic joints. The final joint matrix $\mathbf{H}$ will contain as many columns as the elementary joints composing the complex joint. For example, the joint matrix $\mathbf{H}$ of a spherical joint will contain three columns referred to three non-planar revolute joints. In this case, the joint displacements $\boldsymbol{\theta}_m$ will be composed of three rotations around the axes of the three revolute joints. It is remarked that the assembling order of a complex joint is arbitrary since the proposed formulation is linear and all displacements are considered small.

3.3 Static transformation matrix for mechanisms

Suppose that a system is composed of $n_{\mathcal{J}}$ joint nodes coupled by means of n_c connections and that the number $n_{\mathcal{O}}$ of independent joint nodes can be determined by means of Eq. (8). Following the results obtained in the previous subsection, it is possible to find a system $\mathbf{F}$ of n_c linear constraint equations, defined as:

$$\mathbf{F}(\mathbf{u}_J, \boldsymbol{\theta}_M) = 0, \quad \mathbf{u}_J = \begin{bmatrix} \mathbf{u}_j^{(1)} \\ \mathbf{u}_j^{(2)} \\ \vdots \\ \mathbf{u}_j^{(n_{\mathcal{J}})} \end{bmatrix}, \; \boldsymbol{\theta}_M = \begin{bmatrix} \boldsymbol{\theta}_m^{(1)} \\ \boldsymbol{\theta}_m^{(2)} \\ \vdots \\ \boldsymbol{\theta}_m^{(n_M)} \end{bmatrix} \tag{13}$$

where n_M is the number of mobile connections ($n_M \leq n_c$). Using the linearity of $\mathbf{F}$, it is possible to derive $\mathbf{u}_J$ in function of the vector $\mathbf{u}_O$ of independent joint displacements:

$$\mathbf{u}_J = \mathbf{G}_J \mathbf{u}_O + \mathbf{H}_J \boldsymbol{\theta}_M, \quad \mathbf{u}_O = \begin{bmatrix} \mathbf{u}_o^{(1)} \\ \mathbf{u}_o^{(2)} \\ \vdots \\ \mathbf{u}_o^{(n_{\mathcal{O}})} \end{bmatrix} \tag{14}$$

where $\mathbf{G}_J$ is the $(6 \cdot n_{\mathcal{J}}) \times (6 \cdot n_{\mathcal{O}})$ global matrix of rigid-body transformations and $\mathbf{H}_J$ is the $(6 \cdot n_{\mathcal{J}}) \times n_M$ global joint matrix. Since the set of boundary nodes $\mathcal{B}$ is contained in $\mathcal{J}$, it is possible to extract the vector $\mathbf{u}_\mathrm{B}$ containing all the boundary node displacement vectors from $\mathbf{u}_J$, that is

$$\mathbf{u}_\mathrm{B} = \mathbf{G}_\mathrm{B} \mathbf{u}_O + \mathbf{H}_\mathrm{B} \boldsymbol{\theta}_M \tag{15}$$

where $\mathbf{G}_\mathrm{B}$ is a $(6 \cdot n_{\mathcal{B}}) \times (6 \cdot n_{\mathcal{O}})$ matrix of rigid-body transformations and $\mathbf{H}_\mathrm{B}$ is the $(6 \cdot n_{\mathcal{B}}) \times n_M$ joint matrix. Both matrices refer only to the boundary nodes.

The linearized dynamic equations are similar to those reported in Eq. (1) except for the vector $\mathbf{r}_\mathrm{B}$ of constraint forces due to the joints contribution, i.e.,

$$\begin{bmatrix} \mathbf{M}_\mathrm{II} & \mathbf{M}_\mathrm{IB} \\ \mathbf{M}_\mathrm{BI} & \mathbf{M}_\mathrm{BB} \end{bmatrix} \begin{bmatrix} \ddot{\mathbf{u}}_\mathrm{I} \\ \ddot{\mathbf{u}}_\mathrm{B} \end{bmatrix} + \begin{bmatrix} \mathbf{K}_\mathrm{II} & \mathbf{K}_\mathrm{IB} \\ \mathbf{K}_\mathrm{BI} & \mathbf{K}_\mathrm{BB} \end{bmatrix} \begin{bmatrix} \mathbf{u}_\mathrm{I} \\ \mathbf{u}_\mathrm{B} \end{bmatrix} = \begin{bmatrix} \mathbf{0} \\ \mathbf{f}_\mathrm{B} + \mathbf{r}_\mathrm{B} \end{bmatrix} \tag{16}$$

It is noteworthy that $\mathbf{r}_\mathrm{I} = \mathbf{0}$ since the joints pertain only to the boundary nodes. Following the same approach used in the Guyan–Iron method, we aim to find a novel static transformation matrix including joints. Omitting the acceleration terms, the static equations of the mechanical system become

$$\begin{bmatrix} \mathbf{K}_\mathrm{II} & \mathbf{K}_\mathrm{IB} \\ \mathbf{K}_\mathrm{BI} & \mathbf{K}_\mathrm{BB} \end{bmatrix} \begin{bmatrix} \mathbf{u}_\mathrm{I} \\ \mathbf{u}_\mathrm{B} \end{bmatrix} = \begin{bmatrix} \mathbf{0} \\ \mathbf{f}_\mathrm{B} + \mathbf{r}_\mathrm{B} \end{bmatrix} \tag{17}$$

Combining the latter with Eq. (15), we obtain the following system of three equations:

$$\begin{cases} \mathbf{K}_\mathrm{II} \mathbf{u}_\mathrm{I} + \mathbf{K}_\mathrm{IB} \mathbf{u}_\mathrm{B} = \mathbf{0} \\ \mathbf{K}_\mathrm{BI} \mathbf{u}_\mathrm{I} + \mathbf{K}_\mathrm{BB} \mathbf{u}_\mathrm{B} = \mathbf{f}_\mathrm{B} + \mathbf{r}_\mathrm{B} \\ \mathbf{u}_\mathrm{B} = \mathbf{G}_\mathrm{B} \mathbf{u}_O + \mathbf{H}_\mathrm{B} \boldsymbol{\theta}_M \end{cases} \tag{18}$$

with five unknowns, namely $\mathbf{u}_{\mathrm{I}}, \mathbf{u}_{\mathrm{B}}, \mathbf{u}_O, \mathbf{r}_{\mathrm{B}}$, and $\boldsymbol{\theta}_M$. The vector $\mathbf{r}_b$ of constraint forces has components different from zero along the degrees of constraint of the corresponding joint. For instance, considering the revolute joint of Fig. 4 the corresponding constraint vector $\mathbf{r}_b$, composed of one force and one torque, is normal to the joint vector $\mathbf{h}_b$. On the other hand, it is well known from the *screw theory* that the wrench vector associated with a joint is normal to the corresponding twist vector [2]. For our purposes, $\mathbf{r}_b$ is a wrench vector and $\mathbf{h}_b$ is a twist vector; therefore,

$$\mathbf{h}_b^{\mathrm{T}}\mathbf{r}_b = 0, \quad \forall b \in \mathcal{B} \Rightarrow \mathbf{H}_{\mathrm{B}}^{\mathrm{T}}\mathbf{r}_{\mathrm{B}} = \mathbf{0}. \tag{19}$$

Exploiting the orthogonality property $\mathbf{H}_{\mathrm{B}}^{\mathrm{T}}\mathbf{r}_{\mathrm{B}} = \mathbf{0}$, the system (18) turns into

$$\begin{cases} \mathbf{K}_{\mathrm{II}}\mathbf{u}_{\mathrm{I}} + \mathbf{K}_{\mathrm{IB}}\mathbf{u}_{\mathrm{B}} = \mathbf{0} \\ \mathbf{H}_{\mathrm{B}}^{\mathrm{T}}\mathbf{K}_{\mathrm{BI}}\mathbf{u}_{\mathrm{I}} + \mathbf{H}_{\mathrm{B}}^{\mathrm{T}}\mathbf{K}_{\mathrm{BB}}\mathbf{u}_{\mathrm{B}} = \mathbf{H}_{\mathrm{B}}^{\mathrm{T}}\mathbf{f}_{\mathrm{B}} \\ \mathbf{u}_{\mathrm{B}} = \mathbf{G}_{\mathrm{B}}\mathbf{u}_O + \mathbf{H}_{\mathrm{B}}\boldsymbol{\theta}_M \end{cases} \tag{20}$$

which allows to express all the unknowns $\mathbf{u}_{\mathrm{I}}$, $\mathbf{u}_{\mathrm{B}}$, and $\boldsymbol{\theta}_M$ in function of $\mathbf{u}_O$. In particular, it is possible to derive a new static transformation matrix Ψ_L, such that

$$\begin{bmatrix} \mathbf{u}_{\mathrm{I}} \\ \mathbf{u}_{\mathrm{B}} \end{bmatrix} = \Psi_L \mathbf{u}_O \tag{21}$$

Using Ψ_L, the following reduced system can be derived:

$$\mathbf{M}_L \ddot{\mathbf{u}}_O + \mathbf{K}_L \mathbf{u}_O = \mathbf{F}_L \tag{22}$$

where $\mathbf{M}_L$, $\mathbf{K}_L$, respectively, are the reduced mass and stiffness matrices, defined as

$$\mathbf{M}_L = \Psi_L^{\mathrm{T}}\mathbf{M}\Psi_L, \quad \mathbf{K}_L = \Psi_L^{\mathrm{T}}\mathbf{K}\Psi_L \tag{23}$$

and $\mathbf{F}_L$ is the array of reduced forces. We have reported all symbolic calculations in “Appendix”.

4 Numerical results

In the following, the benchmark example of a two-beam frame and the model of a parallel robot are presented. The proposed examples have the dual function of helping the reader to understand the proposed methodology and to compare the method with the classic Guyan–Iron static reduction.

4.1 Two-beam frame

The first example is chosen as the benchmark for the validation and comparison with the Guyan static reduction method. As shown in Fig. 5, two cantilevered beams are connected by a joint, aligned along the z-axis. The geometrical, inertial, and structural parameters used in this example are reported in Table 1.

First, a superelement of the single beam is created by the Guyan–Iron method. Subsequently, the two superelements are combined by our method in a second reduction process to obtain a reduced model to a single

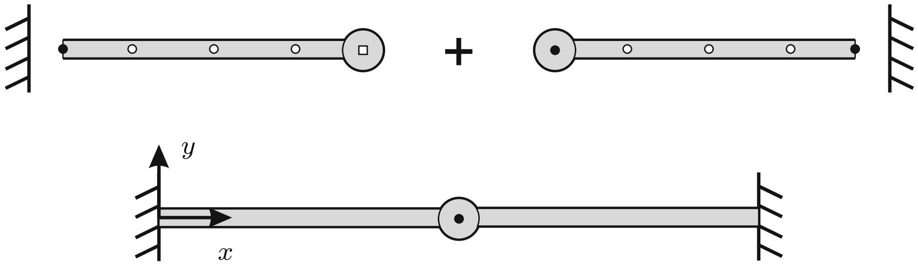

Fig. 5 Two cantilevered beams connected by a revolute joint

Table 1 Geometric and structural parameters of the two-beam frame

Notation	Description	Value	Unit
n	Number of nodes for each link	16	(–)
L	Links' length	1	(m)
b	Base of the cross section	0.025	(m)
h	Height of the cross section	0.025	(m)
E	Young's modulus	200	(GPa)
ν	Poisson's ratio	0.33	(–)
ρ	Material density	7860	(kg/m^3)

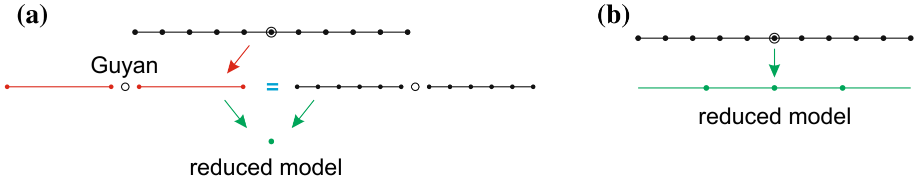

Fig. 6 Subfigure **a** shows the two equivalent approaches that can be used to obtain a reduced model (in this case the 1N model); subfigure **b** shows the reduced model 3N

Table 2 Comparison of the first six natural frequencies (Hz) of three models, with increasing complexity, and ANSYS© results

No.	1N	3N	FN	ANSYS
1	20.00	19.83	20.58	20.36
2	32.93	32.45	32.40	32.37
3	118.70	87.88	86.87	89.11
4	140.88	90.19	89.31	89.11
5	747.26	125.10	128.05	127.23
6	1390.54	179.00	175.02	174.37

central node positioned on the joint. This two-step reduction process is then compared to a single reduction directly obtained by applying the proposed method to the entire system, as shown schematically in the subfigure a) of Fig. 6. We have verified that both the two approaches lead to the same reduced model even if the first approach is faster in terms of computational speed. Carrying out 1000 runs on each approach, we have found that the average time of the first approach varies from 2.9 to 3.1 (ms), while that of the second from 3.5 to 3.7 (ms). This is explained by noting that although the number of input lines is lower in the second approach, the inversion of dimensionally larger matrices slows down the execution of the second approach. From this first analysis, we realize that the method can be applied directly to the starting model or can be applied after the Guyan reduction in the single components. This second strategy is particularly attractive for large-scale systems, where the number of dofs might involve the inversion of large matrices.

We have created two additional models for further analysis. The first model, displayed in the subfigure (b) of Fig. 6, is a reduced model with three nodes (18 dofs): the middle nodes of each beam and the central node at the joint position. This model will be denoted with the name 3N to distinguish it from the previous one-node model, denoted with 1N. Finally, we created a model without reduced inner nodes, i.e., with 174 dofs, denoted with FN. These three models have been compared to ANSYS results, and the first six natural frequencies are reported in Table 2.

As expected, the model 1N fails to capture the internal dynamics of the system and its frequency range is accurate only for the first two values. The 3N model, with the addition of the two central nodes of each beam, is considerably more precise while maintaining a very reduced computational burden. Finally, the third model shows the values closest to those obtained using ANSYS. The computational time takes 4 to 5 (ms) for the 3N model, while the FN model ranges from 23 to 28 (ms), almost one order of magnitude more than the 1N model.

From this analysis, we conclude that our method can be easily combined with the Guyan–Iron method and offers all the advantages and disadvantages of a static method, that is ease of application, reduced use of resources; but also poor precision for low-order models.

4.2 The Ragnar robot

For the second example, the proposed method is applied to the Ragnar robot. Thanks to its architecture and to the use of different end-effector tools, this robot can accomplish either three translations (3T) for pick-and-place tasks or three translations and one rotation (3T1R) [30]. Here, only the 3T solution is studied. In this configuration, each leg of the Ragnar robot has an $RR\Pi R$ architecture with R denoting a revolute joint, while Π denotes a parallelogram joint. The leg layout is shown in Figure 7. A proximal link, with length b, is connected to the base platform $\mathcal{F}$ at point A by means of a revolute joint R of unit vector $\mathbf{e}_A$. The proximal link, in turn, is linked to a parallelogram joint Π by means of a revolute joint with the axis parallel to the unit vector $\mathbf{e}_A$ at the point B. The parallelogram has four revolute joints with axes parallel to the unit vector $\mathbf{e}_\Pi$, and it is composed of two distal links of length l and two short sides of length c. One short side is coupled to the proximal link, while the opposite one is coupled to the moving platform $\mathcal{M}$ by means of a revolute joint of unit vector $\mathbf{e}_A$ at the point C. The first revolute joint at point A is actuated with actuator stiffness identified by k_a. All geometric and inertial parameters that we used for the dynamic reduction are extracted from [30–33] and recalled in Tables 3, 4, and 5 for convenience.

Readers interested in the kinematics and dynamics of the Ragnar robot are referred to [30] for details.

Denoting with P the proximal link of one of the four legs, as shown in Fig. 8, let $P_1 \ldots P_m$ be the nodes after the discretization in three-dimensional beams. Likewise, denoting with D_l and D_r, respectively, the left and right distal links composing the parallelogram, let $D_{l_1} \ldots D_{l_n}$ and $D_{r_1} \ldots D_{r_n}$ be the two series of nodes after the meshing process. Here, the two short sides of the parallelogram and the moving platform $\mathcal{M}$ have been modeled as rigid bodies. It should be remarked that this is only a design choice to show how to couple rigid-to-flexible bodies, and all bodies can thus be modeled as flexible components as well.

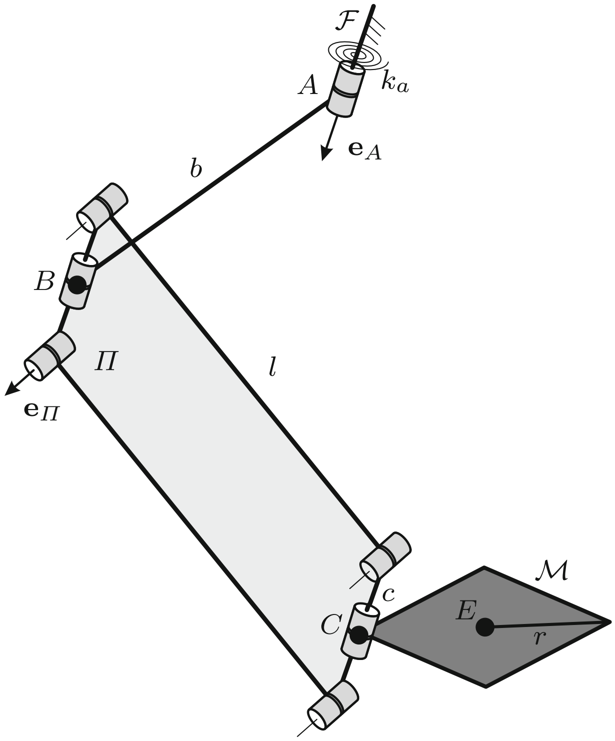

Fig. 7 Leg layout of the Ragnar robot with 3T architecture

Table 3 Design parameters of the Ragnar robot (from Table I of [33])

a_x	a_y	α	β	b	l	r	γ	c
300	100	15°	45°	375	800	100	30°	100

All lengths are expressed in (mm), while the angles are in degrees (°)

Table 4 Material properties (from Table II of [33])

Proximal b (ϕ 60/54 mm)			Distal l (ϕ 16/14 mm)		
E (Gpa)	G (Gpa)	ρ (kg/m^3)	E (Gpa)	G (Gpa)	ρ (kg/m^3)
110	42.31	1600	92	35.4	1600

Table 5 Lumped masses/inertias and actuator stiffness

m_{B} (kg)	m_C (kg)	m_E (kg)	$I_{E_{zz}}$ (kgm^2)	k_a (Nm/rad)
0.7	0.2	2.2	0.026	50,000

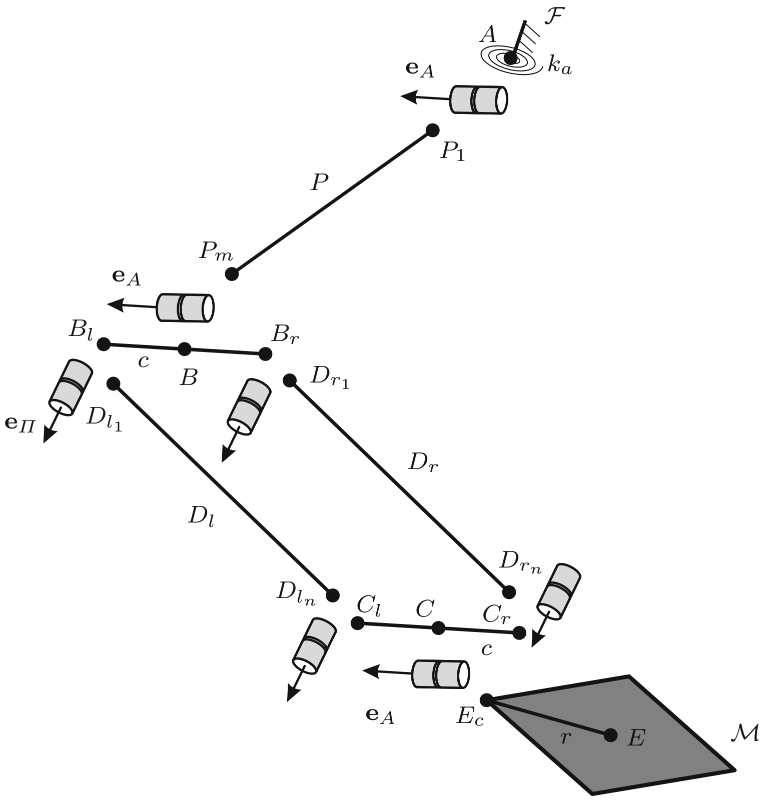

Fig. 8 Leg layout of the Ragnar robot

The leg of the Ragnar robot has been already introduced in Sect. 3.1. It is important to outline that the four legs are not independent but connected to a rigid moving platform $\mathcal{M}$. This connection creates the subsystem shown in Fig. 9 in which, using Eq. (8), only one independent node can be selected. As a matter of fact, this subsystem is given by the assembly of the four subsystems S_3, one for each leg, displayed in Fig. 3. In order to ease the symbolic expressions that will be derived in the following, the central node of the moving platform $\mathcal{M}$, referred to as the end-effector node E, has been selected as the only independent node of the subsystem of Fig. 9. Following what has been described in Sect. 3, the following sets of nodes are defined for each leg:

- inner nodes i: $\{P_2 \ldots P_{m-1}, D_{l_2} \ldots D_{l_{n-1}}, D_{r_2} \ldots D_{r_{n-1}}\}$
- joint nodes j: $\{A, P_1, P_m, B, B_r, B_l, D_{l_1}, D_{l_n}, D_{r_1}, D_{r_n}, C, C_l, C_r, E_c, E\}$
- boundary nodes b: $\{P_1, P_m, D_{l_1}, D_{l_n}, D_{r_1}, D_{r_n}\}$
- independent nodes o: $\{B, E\}$

Notice that the independent nodes refer only to one leg of the robot. Considering that each leg contains one node B and that the node E is in common between the four legs, five independent joint nodes are finally obtained.

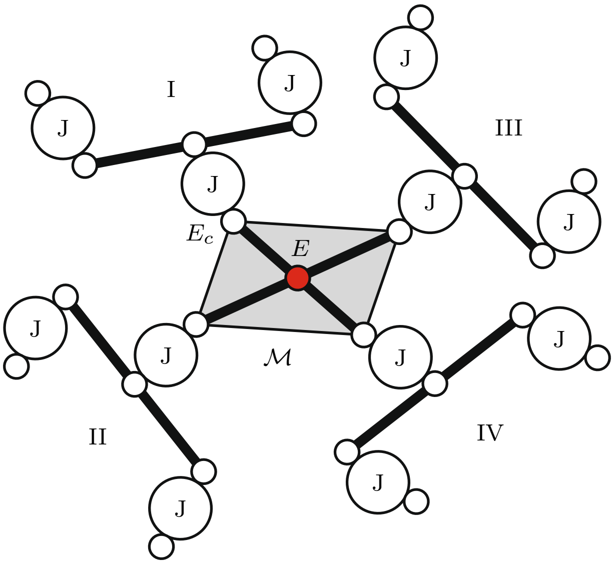

Fig. 9 Robot subsystem composed of the four (I,II,III,IV) leg subsystems S_3 of Fig. 3 and the moving platform $\mathcal{M}$. The end-effector node E (displayed with a red circle) has been identified as the only independent node of the subsystem

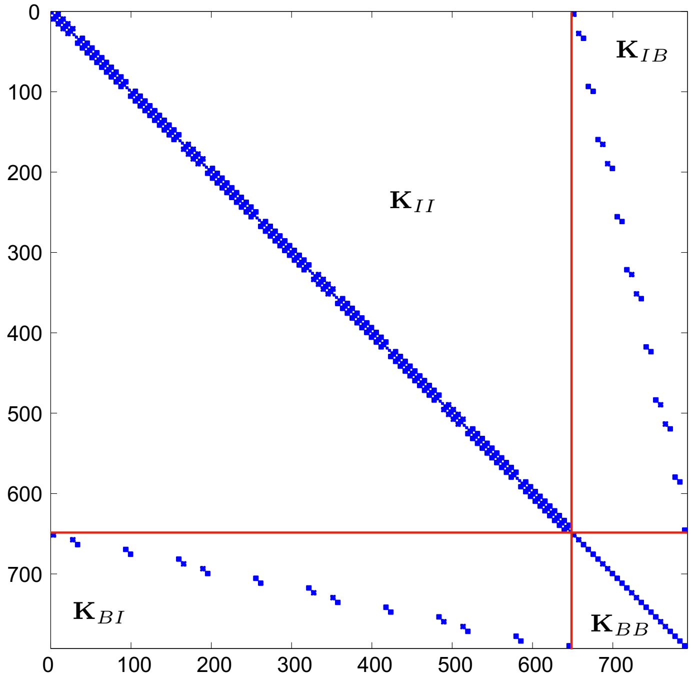

Fig. 10 Stiffness matrix partitioned into blocks of inner and boundary nodes

Here, we used six beams to model the proximal link and 12 elements for each distal link of Π for a total of 792 dofs. After the partitioning into inner and boundary nodes, the stiffness matrix $\mathbf{K}$ of the model appears as shown in Fig.10. The block matrices have been distinguished, and there is no coupling between nodes belonging to different bodies as the joints have not yet been considered.

In the following, the boundary node displacements of one leg will be expressed in terms of the independent node displacements of the same leg. Following the results of Sect. 3.2, the joint vectors $\mathbf{h}$ are defined for all the revolute joints, i.e.,

$$\mathbf{h}_A \equiv \mathbf{h}_\mathrm{B} \equiv \mathbf{h}_C = \begin{bmatrix} \mathbf{0} \\ \mathbf{e}_A \end{bmatrix}, \; \mathbf{h}_\Pi = \begin{bmatrix} \mathbf{0} \\ \mathbf{e}_\Pi \end{bmatrix}. \tag{24}$$

Starting from the boundary nodes of the proximal link, since point A is a point of the base frame $\mathcal{F}$, it follows that the boundary condition $\mathbf{u}_A = \mathbf{0}$ is imposed, resulting in

$$\mathbf{u}_{P_1} = \mathbf{h}_A \theta_A \tag{25a}$$

$$\mathbf{u}_{P_m} = \mathbf{u}_\mathrm{B} + \mathbf{h}_\mathrm{B} \theta_\mathrm{B} \tag{25b}$$

where θ is the rotation of the corresponding revolute joint coming from the deformation of the robot.

Considering the rigid-body assumption, the nodes $\{B_l, B_r\}$ depend on B, while the nodes $\{C_l, C_r\}$ depend on C, that is, in turn, depending on E. For the left and right distal links D_l and D_r, we write

$$\mathbf{u}_{D_{l_1}} = \mathbf{u}_{B_l} + \mathbf{h}_\Pi \theta_{B_l} = \mathbf{G}(+c/2\mathbf{e}_A)\mathbf{u}_B + \mathbf{h}_\Pi \theta_{B_l} \tag{26a}$$

$$\mathbf{u}_{D_{l_n}} = \mathbf{u}_{C_l} + \mathbf{h}_\Pi \theta_{C_l} = \mathbf{G}(+c/2\mathbf{e}_A)\mathbf{u}_C + \mathbf{h}_\Pi \theta_{C_l} \tag{26b}$$

$$\mathbf{u}_{D_{r_1}} = \mathbf{u}_{B_r} + \mathbf{h}_\Pi \theta_{B_r} = \mathbf{G}(-c/2\mathbf{e}_A)\mathbf{u}_B + \mathbf{h}_\Pi \theta_{B_r} \tag{26c}$$

$$\mathbf{u}_{D_{r_n}} = \mathbf{u}_{C_r} + \mathbf{h}_\Pi \theta_{C_r} = \mathbf{G}(-c/2\mathbf{e}_A)\mathbf{u}_C + \mathbf{h}_\Pi \theta_{C_r} \tag{26d}$$

where the rigid-body displacement matrices $\mathbf{G}(\bullet)$ have been defined in Eq. (10). In the previous Eq. (26), the array $\mathbf{u}_C$ can be written in terms of the end-effector array $\mathbf{u}_E$, in fact

$$\mathbf{u}_C = \mathbf{G}(\mathbf{c} - \mathbf{p})\mathbf{u}_E + \mathbf{h}_C \theta_C \tag{27}$$

where $\mathbf{c}$ nd $\mathbf{p}$ are the positioning vectors of points C and E, respectively. By means of Eq. (27), Eq. (26) turns into:

$$\mathbf{u}_{D_{l_1}} = \mathbf{G}(+c/2\mathbf{e}_A)\mathbf{u}_B + \mathbf{h}_\Pi \theta_{B_l} \tag{28a}$$

$$\mathbf{u}_{D_{l_n}} = \mathbf{G}(+c/2\mathbf{e}_A)\mathbf{G}(\mathbf{c} - \mathbf{p})\mathbf{u}_E + \mathbf{G}(+c/2\mathbf{e}_A)\mathbf{h}_C \theta_C + \mathbf{h}_\Pi \theta_{C_l} \tag{28b}$$

$$\mathbf{u}_{D_{r_1}} = \mathbf{G}(-c/2\mathbf{e}_A)\mathbf{u}_B + \mathbf{h}_\Pi \theta_{B_r} \tag{28c}$$

$$\mathbf{u}_{D_{r_n}} = \mathbf{G}(-c/2\mathbf{e}_A)\mathbf{G}(\mathbf{c} - \mathbf{p})\mathbf{u}_E + \mathbf{G}(-c/2\mathbf{e}_A)\mathbf{h}_C \theta_C + \mathbf{h}_\Pi \theta_{C_r}. \tag{28d}$$

Then, noting that $\mathbf{G}(+c/2\mathbf{e}_A)\mathbf{G}(\mathbf{c} - \mathbf{p}) \equiv \mathbf{G}(\mathbf{c}_l - \mathbf{p})$ and $\mathbf{G}(-c/2\mathbf{e}_A)\mathbf{G}(\mathbf{c} - \mathbf{p}) \equiv \mathbf{G}(\mathbf{c}_r - \mathbf{p})$, we finally combine Eqs. (25) and (28) to obtain the same form of Eq. (15), i.e.,

$$\mathbf{u}_\mathrm{B} = \mathbf{G}_\mathrm{B}\mathbf{u}_O + \mathbf{H}_\mathrm{B}\boldsymbol{\theta}_M \tag{29}$$

where the arrays $\mathbf{u}_\mathrm{B}$, $\mathbf{u}_O$ and $\boldsymbol{\theta}_M$ are:

$$\mathbf{u}_\mathrm{B} = \begin{bmatrix} \mathbf{u}_{P_1} \\ \mathbf{u}_{P_m} \\ \mathbf{u}_{D_{l_1}} \\ \mathbf{u}_{D_{l_n}} \\ \mathbf{u}_{D_{r_1}} \\ \mathbf{u}_{D_{r_n}} \end{bmatrix}, \; \mathbf{u}_O = \begin{bmatrix} \mathbf{u}_\mathrm{B} \\ \mathbf{u}_E \end{bmatrix}, \; \boldsymbol{\theta}_M = \begin{bmatrix} \theta_A \\ \theta_{B_l} \\ \theta_B \\ \theta_{B_r} \\ \theta_{C_l} \\ \theta_C \\ \theta_{C_r} \end{bmatrix} \tag{30}$$

while $\mathbf{G}_\mathrm{B}$ is a (36 × 12) matrix and $\mathbf{H}_\mathrm{B}$ is a (36 × 7) matrix, defined as

$$\mathbf{G}_\mathrm{B} = \begin{bmatrix} \mathbf{O} & \mathbf{O} \\ \mathbf{1} & \mathbf{O} \\ \mathbf{G}(+c/2\mathbf{e}_A) & \mathbf{O} \\ \mathbf{O} & \mathbf{G}(\mathbf{c}_l - \mathbf{p}) \\ \mathbf{G}(-c/2\mathbf{e}_A) & \mathbf{O} \\ \mathbf{O} & \mathbf{G}(\mathbf{c}_r - \mathbf{p}) \end{bmatrix} \tag{31}$$

$$\mathbf{H}_\mathrm{B} = \begin{bmatrix} \mathbf{h}_A & \mathbf{0} & \mathbf{0} & \mathbf{0} & \mathbf{0} & \mathbf{0} & \mathbf{0} \\ \mathbf{0} & \mathbf{0} & \mathbf{h}_\mathrm{B} & \mathbf{0} & \mathbf{0} & \mathbf{0} & \mathbf{0} \\ \mathbf{0} & \mathbf{h}_\Pi & \mathbf{0} & \mathbf{0} & \mathbf{0} & \mathbf{0} & \mathbf{0} \\ \mathbf{0} & \mathbf{0} & \mathbf{0} & \mathbf{0} & \mathbf{h}_\Pi & \mathbf{G}(+c/2\mathbf{e}_A)\mathbf{h}_C & \mathbf{0} \\ \mathbf{0} & \mathbf{0} & \mathbf{0} & \mathbf{h}_\Pi & \mathbf{0} & \mathbf{0} & \mathbf{0} \\ \mathbf{0} & \mathbf{0} & \mathbf{0} & \mathbf{0} & \mathbf{0} & \mathbf{G}(-c/2\mathbf{e}_A)\mathbf{h}_C & \mathbf{h}_\Pi \end{bmatrix}. \tag{32}$$

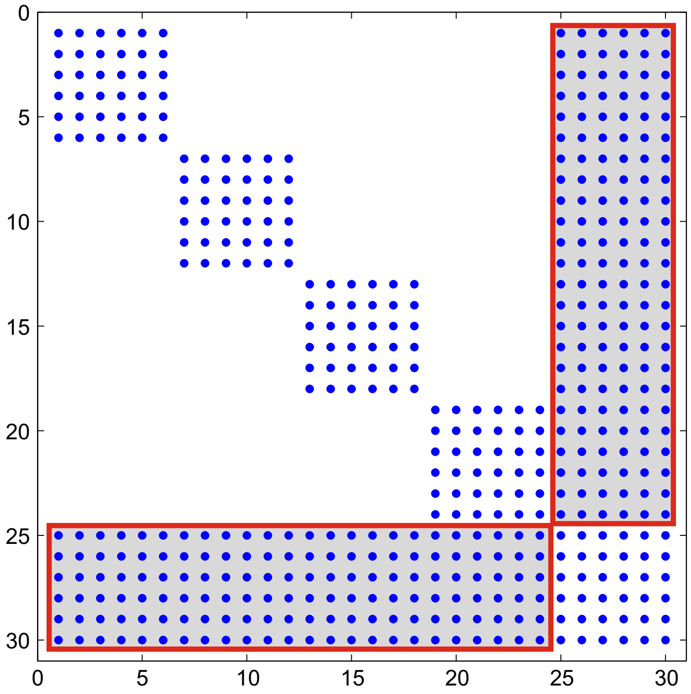

Fig. 11 Stiffness matrix of the reduced model: the four nodes B of the legs are coupled to the end-effector node E by means of off-diagonal block matrices highlighted in grayed boxes

The expressions of $\mathbf{G}_\mathrm{B}$ and $\mathbf{H}_\mathrm{B}$ are referred to the generic leg and must be assembled to create the matrices of the global model. The assembly procedure, not reported here for brevity, can be carried out following common FE techniques.

The elastic wrench $\mathbf{w}_a$ coming from the actuator stiffness k_a has the following expression reported in "Appendix":

$$\mathbf{w}_a = -k_a \mathbf{h}_A \theta_A \equiv -\mathbf{K}_E \mathbf{H}_\mathrm{B} \boldsymbol{\theta}_M, \quad \mathbf{K}_E = \mathrm{diag}(k_a \mathbf{1}_6, \mathbf{O}_6, \mathbf{O}_6, \mathbf{O}_6, \mathbf{O}_6, \mathbf{O}_6). \tag{33}$$

The actuator stiffness matrix $\mathbf{K}_E$ is then used to obtain θ_M from Eq. (46) and $\mathbf{L}_\mathrm{B}$ from Eq. (39). For the following results, we considered that $\mathbf{f}_\mathrm{B} = \mathbf{0}$ and $\mathbf{L}_F = \mathbf{O}$ in Eq. (39). Using $\mathbf{L}_\mathrm{B}$, the reduced stiffness matrix $\mathbf{K}_L$ can be obtained. The latter includes the dofs of five nodes, respectively, the four nodes at points B of each leg and the end-effector node E of the moving platform $\mathcal{M}$, for a total of 30 dofs. As shown in Fig. 11, the shape of $\mathbf{K}_L$ reflects the robot architecture: Four diagonal blocks pertain to the nodes B of the legs and are decoupled among them and coupled to the last diagonal block of node E through off-diagonal blocks.

It is important to remark that when a mechanism changes its posture, its stiffness and mass matrices, and the joints vectors must be updated. Nevertheless, unless the system changes topology with the introduction or removal of some kinematic chain, the symbolic expression of the reduction matrix $\mathbf{L}_\mathrm{B}$ will remain the same.

Sometimes, designers are interested only in the stiffness matrix reduced to a specific point, for instance the end-effector point E of the Ragnar robot, usually referred to as the Cartesian stiffness matrix. In our formulation, this is easily obtained by means of a second Guyan–Iron reduction applied to the dofs of $\mathbf{K}_L$. In this second reduction, the nodes to be condensed are considered as the inner nodes in a similar way to the classic static reduction applied to structures. For the Ragnar robot, the four nodes B are considered inner nodes, while the node E remains the only boundary node.

The reduced mass matrix $\mathbf{M}_L$ follows the same transformation of $\mathbf{K}_L$, but lumped mass/inertia and the way to include it in the model are worthy of particular attention. Lumped masses can be added both to inner and boundary nodes. For instance, the lumped masses at nodes B and E are added directly to the final $\mathbf{M}_L$ since the independent nodes B and E do not appear among the initial inner and boundary nodes. Finally, to take into account the mass at the joint node C this must first be referred to the independent node E by means of the following expression derived from the kinetic energy equivalence:

$$\mathbf{M}_{CE} = \mathbf{G}(\mathbf{c} - \mathbf{p})^\mathrm{T} \mathbf{M}_C \mathbf{G}(\mathbf{c} - \mathbf{p}). \tag{34}$$

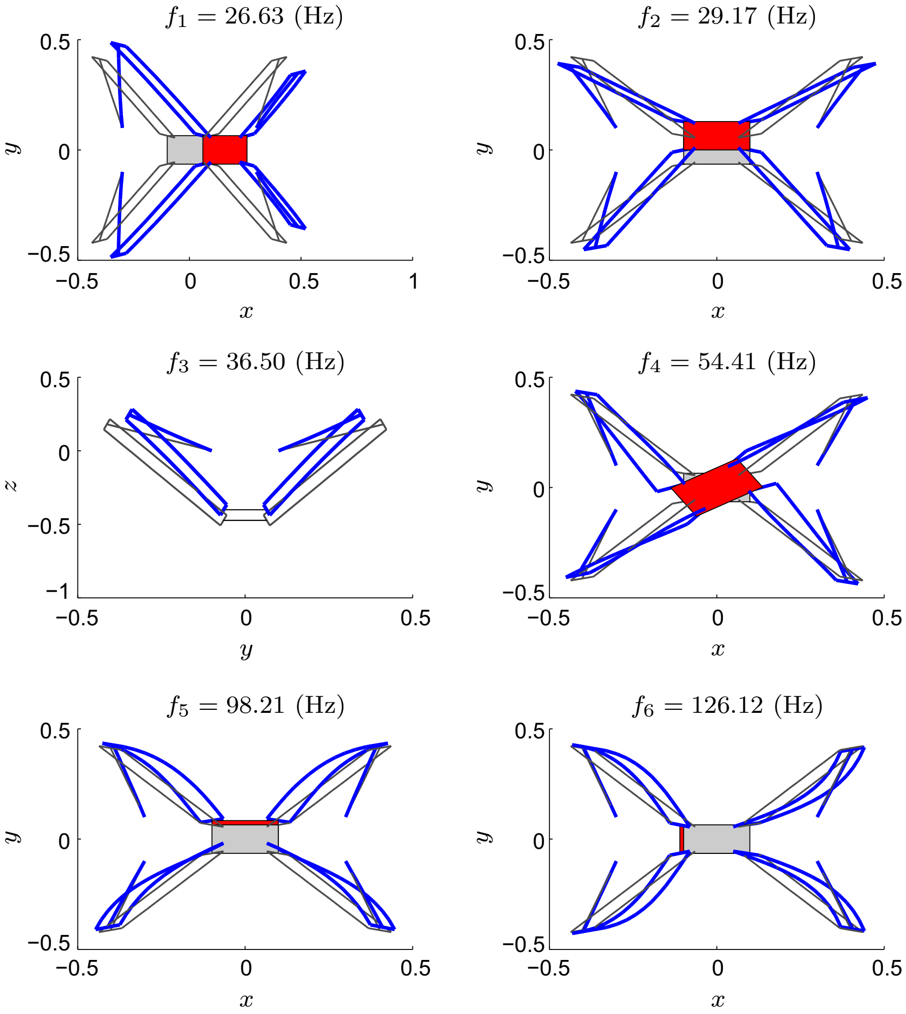

Fig. 12 The first six modes of the Ragnar robot calculated at $\mathbf{p} = [0, 0, -0.5]$ (m). The starting undeformed configuration is superimposed on the mode shape

The latter can be added to the corresponding dofs of E in the final $\mathbf{M}_L$. The shape of $\mathbf{M}_L$ is similar to that of $\mathbf{K}_L$, shown in Fig. 11, and it is not reported for brevity.

To report some feasible results, the natural frequency and modes have been calculated when point E is individuated by the positioning vector $\mathbf{p} = [0, 0, -0.5]$ (m). This configuration has been chosen to help the reader to understand the modes and to identify the planes of symmetry.

Figure 12 plots the first six modes. It can be observed that the first three modes pertain to the three degrees of freedom of the Ragnar robot, i.e., the three rigid translations along the directions of x, y and z, respectively. It is worthy of attention that the first two modes follow the rectangular symmetry of the robot; in fact, the points A are positioned at the vertices of a rectangle. From the fourth mode onward, the modes involve deformations of the legs. In particular, the fourth mode is a rotation around the z-axis that reveals low z-rotational stiffness of the robot. This is confirmed by the Cartesian stiffness matrix $\mathbf{K}_{L_E}$ obtained after a second static reduction to the end-effector point E, i.e.,

$$\mathbf{K}_{L_E} = 10^5 \cdot \begin{bmatrix} 1.5597 & 0 & 0 & 0 & -0.2524 & 0 \\ 0 & 2.0619 & 0 & 0.1683 & 0 & 0 \\ 0 & 0 & 7.2343 & 0 & 0 & 0 \\ 0 & 0.1683 & 0 & 0.1760 & 0 & 0 \\ -0.2524 & 0 & 0 & 0 & 0.5614 & 0 \\ 0 & 0 & 0 & 0 & 0 & 0.0466 \end{bmatrix}.$$

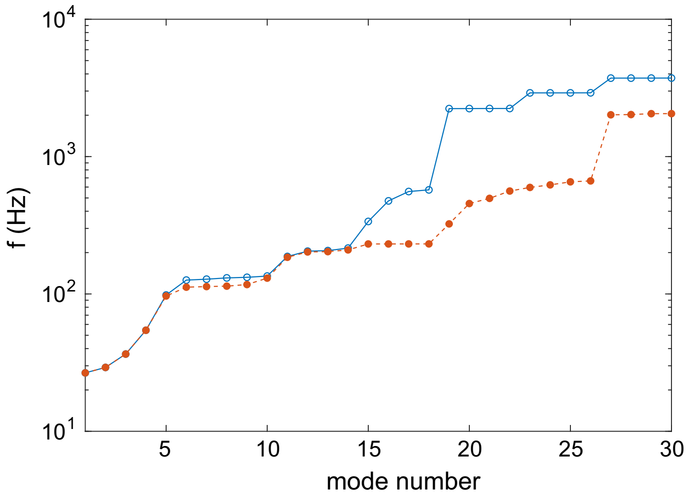

Fig. 13 The first 30 natural frequencies (Hz) of the Ragnar robot at $\mathbf{p} = [0, 0, -0.5]$ (m). The reduced model is plotted with solid line and markers with blank circles, and the full model is plotted with dashed line and dotted markers

As it can be observed, the z-rotational stiffness is one order of magnitude lower than the x- and y-rotational stiffness. For the sake of completeness, the Cartesian mass matrix $\mathbf{M}_{L_E}$ is also reported.

$$\mathbf{M}_{L_E} = \begin{bmatrix} 5.3821 & 0 & 0 & 0 & -0.3594 & 0 \\ 0 & 5.9435 & 0 & 0.235 & 0 & 0 \\ 0 & 0 & 13.4442 & 0 & 0 & 0 \\ 0 & 0.2350 & 0 & 0.0505 & 0 & 0 \\ -0.3594 & 0 & 0 & 0 & 0.0979 & 0 \\ 0 & 0 & 0 & 0 & 0 & 0.0397 \end{bmatrix}.$$

The previous Cartesian matrices reveal that the method is perfectly integrated with other static substructuring methods. Unlike the previous two-beam example, we used the Guyan method for a second reduction necessary to condense all boundary dofs into a single node.

Figure 13 shows the first 30 natural frequencies for the full model, i.e., without reduction, and for the reduced model. It can be observed that the two models are similar in the low-frequency range, while the differences become wider for high frequencies. This behavior is not surprising as it is typical of static CMS methods.

We finally show in Fig. 14 four mesh plots of the first four natural frequencies evaluated on a rectangular workspace of 480 × 900 (mm^2) and with fixed height $p_z = -570$ (mm). It is interesting to note how the frequencies are more influenced by the x- than the y-coordinate and how the performances decay at the edges of the chosen workspace.

5 Conclusions

The classic Guyan–Iron reduction has been extended to mechanisms combining the linear structural dynamics to FE/MSA. Compatibility conditions have been written by means of a new class of joint nodes completing the existing classes of inner and boundary nodes, already used in static reduction techniques. We demonstrated that only a reduced set of independent joint nodes can be identified and a simple connection rule has been defined to select the independent joint nodes of a mechanical system composed of rigid parts, flexible parts, and joints. The compatibility conditions and the governing statics equations have been combined to find a static transformation matrix. The new transformation matrix maintains a form similar to the Guyan–Iron transformation matrix. Actuation stiffness and external nodal forces have been also considered to obtain the final reduced model. The formulation has been first applied to a two-beam frame chosen as benchmark example. We have verified that the proposed method can be perfectly integrated with the Guyan–Iron reduction method. Then, we applied the method to the Ragnar robot, a commercial pick-and-place parallel robot. In this second example, rigid and flexible bodies have been combined together with joints to provide a complex elastodynamic system. The novel formulation offers a global treatment of the couplings and is highly flexible allowing to obtain concise models with a reduced

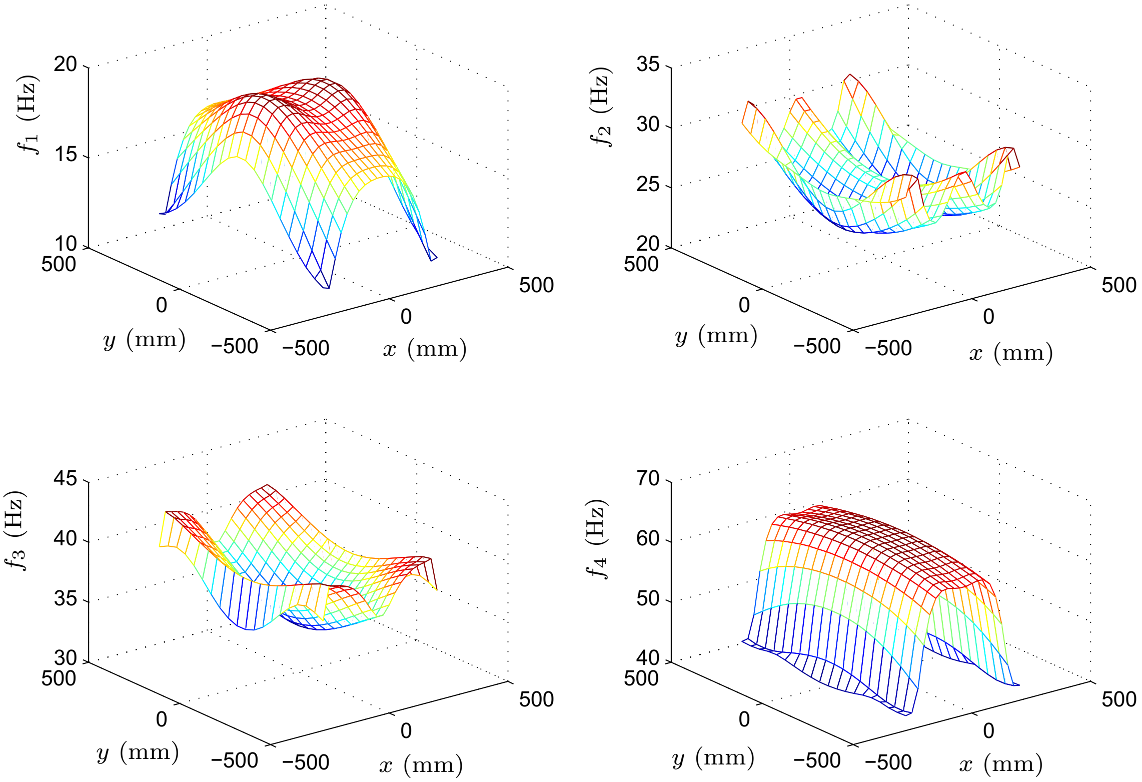

Fig. 14 The first four natural frequencies (Hz) on a rectangular workspace of 480 × 900 (mm^2) and with fixed height $p_z = -570$ (mm)

number of dofs. Besides, imposed motions and boundary conditions can be directly included in the definition of the joint constraints. The proposed method does not replace the classic static methods but aims to be integrated and combined with them in order to create a unique substructuring framework. When considering problems with large-scale components, it is possible to make a first static reduction on the individual components and then apply the proposed method on the reduced system. Vice versa, it is possible to do the opposite making a second static reduction after a primary reduction carried out through our method, as performed in the Ragnar robot example to find the stiffness and mass Cartesian matrices of the robot. Therefore, the method combines the existing techniques and is an enhancement when one wants to create superelements with joints condensed inside.

Acknowledgements The authors declare that they have no conflict of interest.

Appendix

In Sect. 3.3, the following system (20) has been derived:

$$\begin{cases} \mathbf{K}_{\mathrm{II}}\mathbf{u}_{\mathrm{I}} + \mathbf{K}_{\mathrm{IB}}\mathbf{u}_{\mathrm{B}} = \mathbf{0} \\ \mathbf{H}_{\mathrm{B}}^{\mathrm{T}}\mathbf{K}_{\mathrm{BI}}\mathbf{u}_{\mathrm{I}} + \mathbf{H}_{\mathrm{B}}^{\mathrm{T}}\mathbf{K}_{\mathrm{BB}}\mathbf{u}_{\mathrm{B}} = \mathbf{H}_{\mathrm{B}}^{\mathrm{T}}\mathbf{f}_{\mathrm{B}} \\ \mathbf{u}_{\mathrm{B}} = \mathbf{G}_{\mathrm{B}}\mathbf{u}_{O} + \mathbf{H}_{\mathrm{B}}\boldsymbol{\theta}_{M} \end{cases} \tag{35}$$

It can be recognized that from the first equation of this system, the Guyan–Iron transformation is recovered. Then, after substituting the third equation into the second one, we derive

$$\mathbf{H}_{\mathrm{B}}^{\mathrm{T}}\mathbf{K}_{\mathrm{BI}}\mathbf{u}_{\mathrm{I}} + \mathbf{H}_{\mathrm{B}}^{\mathrm{T}}\mathbf{K}_{\mathrm{BB}}\mathbf{G}_{\mathrm{B}}\mathbf{u}_{O} + \mathbf{H}_{\mathrm{B}}^{\mathrm{T}}\mathbf{K}_{\mathrm{BB}}\mathbf{H}_{\mathrm{B}}\boldsymbol{\theta}_{M} = \mathbf{H}_{\mathrm{B}}^{\mathrm{T}}\mathbf{f}_{\mathrm{B}} \tag{36}$$

After computation, $\boldsymbol{\theta}_M$ is obtained, i.e.,

$$\boldsymbol{\theta}_{M} = -(\mathbf{H}_{\mathrm{B}}{}^{\mathrm{T}}\mathbf{K}_{\mathrm{BB}}\mathbf{H}_{B})^{-1}(\mathbf{H}_{\mathrm{B}}{}^{\mathrm{T}}\mathbf{K}_{\mathrm{BI}}\mathbf{u}_{\mathrm{I}} + \mathbf{H}_{\mathrm{B}}^{\mathrm{T}}\mathbf{K}_{\mathrm{BB}}\mathbf{G}_{B}\mathbf{u}_{O} - \mathbf{H}_{\mathrm{B}}^{\mathrm{T}}\mathbf{f}_{B}). \tag{37}$$

Substituting $\boldsymbol{\theta}_M$ into the third equation of the system, we finally obtain

$$\mathbf{u}_\mathrm{B} = \mathbf{L}_\mathrm{B}\mathbf{u}_O + \mathbf{L}_F\mathbf{f}_\mathrm{B} \tag{38}$$

where

$$\begin{aligned}
\mathbf{L}_F &= \boldsymbol{\Gamma}_\mathrm{B}^{-1}(\mathbf{H}_B {\Delta_\mathrm{B}}^{-1}{\mathbf{H}_B}^\mathrm{T}) && (39a)\\
\mathbf{L}_\mathrm{B} &= \boldsymbol{\Gamma}_\mathrm{B}^{-1}(\mathbf{H}_B {\Delta_\mathrm{B}}^{-1}{\mathbf{H}_B}^\mathrm{T}\mathbf{K}_\mathrm{BB}\mathbf{G}_\mathrm{B} - \mathbf{G}_\mathrm{B}) && (39b)\\
\boldsymbol{\Gamma}_\mathrm{B} &= \mathbf{H}_B {\Delta_\mathrm{B}}^{-1}{\mathbf{H}_B}^\mathrm{T}\mathbf{K}_\mathrm{BI}{\mathbf{K}_\mathrm{II}}^{-1}\mathbf{K}_\mathrm{IB} - \mathbf{1}_\mathrm{B} && (39c)
\end{aligned}$$

and $\Delta_\mathrm{B} = {\mathbf{H}_\mathrm{B}}^\mathrm{T}\mathbf{K}_\mathrm{BB}\mathbf{H}_B$. Without changing the sense of the explanation, let us impose $\mathbf{f}_\mathrm{B} = \mathbf{0}$, and then, the expression between $\mathbf{u}_\mathrm{B}$ and $\mathbf{u}_O$ is reduced to

$$\mathbf{u}_\mathrm{B} = \mathbf{L}_\mathrm{B}\mathbf{u}_O \tag{40}$$

where $\mathbf{L}_\mathrm{B}$ is used to create a new transformation matrix Ψ_L, defined as

$$\begin{bmatrix} \mathbf{u}_\mathrm{I} \\ \mathbf{u}_\mathrm{B} \end{bmatrix} = \Psi_L\mathbf{u}_O \Rightarrow \Psi_L = \Psi\mathbf{L}_\mathrm{B} \tag{41}$$

where Ψ has been defined in Eq. (4) for the Guyan–Iron condensation. It can be verified by direct substitution that when all joints are locked, that is when $\mathbf{H}_B \equiv \mathbf{O}$, it follows that $\mathbf{L}_\mathrm{B} \equiv \mathbf{G}_\mathrm{B}$ and $\Psi_L \equiv \Psi\mathbf{G}_\mathrm{B}$. The latter expresses that the Guyan–Iron transformation can be recovered simply by blocking the joints. Considering Ψ_L, the following reduced system is written

$$\mathbf{M}_L\ddot{\mathbf{u}}_b + \mathbf{K}_L\mathbf{u}_b = \mathbf{F}_L \tag{42}$$

where $\mathbf{M}_L$, $\mathbf{K}_L$, respectively, are the reduced mass and stiffness matrices, defined as

$$\mathbf{M}_L = \Psi_L^\mathrm{T}\mathbf{M}\Psi_L, \quad \mathbf{K}_L = \Psi_L^\mathrm{T}\mathbf{K}\Psi_L \tag{43}$$

and $\mathbf{F}_L$ is the array of reduced forces. The expressions of $\mathbf{M}_L$, $\mathbf{K}_L$ and $\mathbf{F}_L$ are not reported for brevity. Compared to the previous formulations proposed by the authors in [4,6,7], the new approach is *global* and does not require different cases of coupling between bodies.

In particular cases, the vector $\mathbf{f}_\mathrm{B}$ may include elastic forces. Therefore, suppose that an elastic force/torque is applied to the boundary node of a generic joint, the corresponding generalized force vector $\mathbf{f}_b$ becomes

$$\mathbf{f}_b = -k_e\mathbf{h}_b\theta_m \tag{44}$$

where k_e is the stiffness at the joint location. This expression can be extended to the global vector $\mathbf{f}_\mathrm{B}$, i.e.,

$$\mathbf{f}_\mathrm{B} = -\mathbf{K}_E\mathbf{H}_\mathrm{B}\boldsymbol{\theta}_M, \quad \mathbf{K}_E = \mathrm{diag}(\mathbf{O}_6, \ldots, k_e\mathbf{1}_6, \ldots, \mathbf{O}_6) \tag{45}$$

where $\mathbf{K}_E$ is the generalized stiffness matrix containing all joint stiffness. By substituting this expression into the right-side term $\mathbf{H}_\mathrm{B}^\mathrm{T}\mathbf{f}_\mathrm{B}$ of Eq. (36), we obtain

$$\mathbf{H}_\mathrm{B}^\mathrm{T}\mathbf{K}_\mathrm{BI}\mathbf{u}_\mathrm{I} + \mathbf{H}_\mathrm{B}^\mathrm{T}\mathbf{K}_\mathrm{BB}\mathbf{G}_\mathrm{B}\mathbf{u}_O + \mathbf{H}_\mathrm{B}^\mathrm{T}\mathbf{K}_\mathrm{BB}\mathbf{H}_\mathrm{B}\boldsymbol{\theta}_M = -\mathbf{H}_\mathrm{B}^\mathrm{T}\mathbf{K}_E\mathbf{H}_\mathrm{B}\boldsymbol{\theta}_M \tag{46}$$

from which it can be obtained that $\boldsymbol{\theta}_M$ becomes

$$\boldsymbol{\theta}_M = -[{\mathbf{H}_\mathrm{B}}^\mathrm{T}(\mathbf{K}_\mathrm{BB} + \mathbf{K}_E)\mathbf{H}_B]^{-1}({\mathbf{H}_\mathrm{B}}^\mathrm{T}\mathbf{K}_\mathrm{BI}\mathbf{u}_\mathrm{I} + \mathbf{H}_\mathrm{B}^\mathrm{T}\mathbf{K}_\mathrm{BB}\mathbf{G}_B\mathbf{u}_O) \tag{47}$$

This expression replaces Eq. (37) and allows for obtaining the transformation matrix Ψ_L in a manner similar to what has been done previously.

References

1. Alessandro, C., Rosario, S.: Elastodynamic optimization of a 3t1r parallel manipulator. Mech. Mach. Theory **73**, 184–196 (2014)
2. Angeles, J., Angeles, J.: Fundamentals of robotic mechanical systems: theory. Methods, and Algorithms (Mechanical Engineering Series, Vol. 2) p. 98 (2007)
3. Bai, Z., Su, Y.: Dimension reduction of large-scale second-order dynamical systems via a second-order Arnoldi method. SIAM J. Sci. Comput. **26**(5), 1692–1709 (2005)
4. Cammarata, A.: Unified formulation for the stiffness analysis of spatial mechanisms. Mech. Mach. Theory **105**, 272–284 (2016)
5. Cammarata, A.: A novel method to determine position and orientation errors in clearance-affected overconstrained mechanisms. Mech. Mach. Theory **118**, 247–264 (2017)
6. Cammarata, A., Condorelli, D., Sinatra, R.: An algorithm to study the elastodynamics of parallel kinematic machines with lower kinematic pairs. J. Mech. Robot. **5**(1), 011004 (2013)
7. Cammarata, A., D'Urso, D., Caliò, I., Greco, A., Lacagnina, M., Fichera, G.: Dynamic stiffness model of spherical parallel robots. J. Sound Vib. **384**, 312–324 (2016)
8. Cammarata, A., Sinatra, R.: On the elastostatics of spherical parallel machines with curved links. In: Recent Advances in Mechanism Design for Robotics, pp. 347–356. Springer, Berlin (2015)
9. Cardona, A., Géradin, M.: A superelement formulation for mechanism analysis. Comput. Methods Appl. Mech. Eng. **100**(1), 1–29 (1992)
10. Castanier, M.P., Tan, Y.C., Pierre, C.: Characteristic constraint modes for component mode synthesis. AIAA J. **39**(6), 1182–1187 (2001)
11. Chen, S.H., Pan, H.: Guyan reduction. Int. J. Numer. Methods Biomed. Eng. **4**(4), 549–556 (1988)
12. Gawronski, W.K.: Dynamics and Control of Structures: A Modal Approach. Springer, Berlin (2004)
13. Guyan, R.J.: Reduction of stiffness and mass matrices. AIAA J. **3**(2), 380 (1965)
14. Herting, D.: A general purpose, multi-stage, component modal synthesis method. Finite Elem. Anal. Des. **1**(2), 153–164 (1985)
15. Hinke, L., Dohnal, F., Mace, B.R., Waters, T.P., Ferguson, N.: Component mode synthesis as a framework for uncertainty analysis. J. Sound Vib. **324**(1), 161–178 (2009)
16. Hurty, W.C.: Dynamic analysis of structural systems using component modes. AIAA J. **3**(4), 678–685 (1965)
17. Klerk, Dd, Rixen, D.J., Voormeeren, S.: General framework for dynamic substructuring: history, review and classification of techniques. AIAA J. **46**(5), 1169–1181 (2008)
18. Lall, S., Marsden, J.E., Glavaški, S.: A subspace approach to balanced truncation for model reduction of nonlinear control systems. Int. J. Robust Nonlinear Control IFAC Affil. J. **12**(6), 519–535 (2002)
19. Leung, A.Y.T.: An accurate method of dynamic condensation in structural analysis. Int. J. Numer. Methods Eng. **12**(11), 1705–1715 (1978)
20. MacNeal, R.H.: A hybrid method of component mode synthesis. Comput. Struct. **1**(4), 581–601 (1971)
21. Murray-Smith, R., Johansen, T.: Multiple Model Approaches to Nonlinear Modelling and Control. CRC Press, Boca Raton (1997)
22. Qiu, J.B., Ying, Z.G., Williams, F.: Exact modal synthesis techniques using residual constraint modes. Int. J. Numer. Methods Eng. **40**(13), 2475–2492 (1997)
23. Qu, Z.Q.: Model Order Reduction Techniques with Applications in Finite Element Analysis. Springer, Berlin (2013)
24. Rixen, D.J.: A dual craig–bampton method for dynamic substructuring. J. Comput. Appl. Math. **168**(1–2), 383–391 (2004)
25. Rubin, S.: Improved component-mode representation for structural dynamic analysis. AIAA J. **13**(8), 995–1006 (1975)
26. Scherer, C.W.: LPV control and full block multipliers. Automatica **37**(3), 361–375 (2001)
27. Shabana, A.A., Wehage, R.A.: A coordinate reduction technique for dynamic analysis of spatial substructures with large angular rotations. J. Struct. Mech. **11**(3), 401–431 (1983)
28. Su, T.J., Craig, R.R.: Model reduction and control of flexible structures using Krylov vectors. J. Guidance Control Dyn. **14**(2), 260–267 (1991)
29. Wittrick, W., Williams, F.: A general algorithm for computing natural frequencies of elastic structures. Q. J. Mech. Appl. Math. **24**(3), 263–284 (1971)
30. Wu, G., Bai, S., Hjørnet, P.: Design analysis and dynamic modeling of a high-speed 3t1r pick-and-place parallel robot. In: Recent Advances in Mechanism Design for Robotics, pp. 285–295. Springer, Berlin (2015)
31. Wu, G., Bai, S., Hjørnet, P.: Parametric optimal design of a parallel schönflies-motion robot under pick-and-place trajectory constraints. In: Intelligent Robots and Systems (IROS), 2015 IEEE/RSJ International Conference on, pp. 3158–3163. IEEE (2015)
32. Wu, G., Bai, S., Hjørnet, P.: Multi-objective design optimization of a parallel schönflies-motion robot. In: Advances in Reconfigurable Mechanisms and Robots II, pp. 657–667. Springer, Berlin (2016)
33. Wu, G., Bai, S., Hjørnet, P.: On the stiffness of three/four degree-of-freedom parallel pick-and-place robots with four identical limbs. In: 2016 IEEE International Conference on Robotics and Automation (ICRA), pp. 861–866. IEEE (2016)

Publisher's Note Springer Nature remains neutral with regard to jurisdictional claims in published maps and institutional affiliations.